

Static Characteristic Analysis of Spatial (Non-Planar) Links in Planar Parallel Manipulator

M. Ganesh* , Anjan Kumar Dash, P. Venkitachalam and S. Shrinithi

School of Mechanical Engineering, SASTRA University, Thanjavur 613 402, India.
E-mails: anjandash@mech.sastra.edu, urpalvenki@gmail.com, shrinithi3@gmail.com

(Accepted April 4, 2020. First published online: May 6, 2020)

SUMMARY

Conventional planar manipulators have their links in a single plane. Increasing payload at the end effector/mobile platform can induce high stress in the links due to the cantilever nature of links. Thus, it limits the total vertical load that can be applied on the mobile platform. In contrast to the links in conventional planar parallel mechanisms, non-planar links are proposed in this paper, that is, links are made inclined to the horizontal plane and non-planar legs are constructed. Though the links are made non-planar, the end effectors' planar motion is retained. For studying the application of such non-planar links in planar manipulators, new models of inertia, stiffness and leg dynamics have to be developed. In this article, these models are developed by the static analysis of the planar manipulators with non-planar links, and the performance is compared with the corresponding conventional planar manipulators.

KEYWORDS: 3- \bar{R} RR planar parallel robot; Moment of Inertia; Stiffness analysis and optimization.

1. Introduction

Parallel robots have been under intensive study for over one decade. Unlike the serial manipulator, a parallel manipulator consists of several independent chains, an end effector and a base platform forming a closed-loop kinematic chain. It is well known that parallel kinematic structures offer advantages, such as high accuracy, payload-to-weight ratio, high natural frequencies and rigidity compared to serial manipulators. Of the parallel manipulators, 3-degrees of freedom (DOF) planar parallel manipulators are widely used as parallel kinematic machine.^{1,2} Hence, it has attracted many researchers to study on its workspace, direct kinematics, kinematic synthesis and analysis assembly modes, singularity analysis, static forces, dimensional synthesis, optimal design and dynamics.^{3–16}

Planar manipulators find its application in fast positioning or assembly operations. Such applications make use of the high-speed capability with minimum positioning error, large stiffness and low inertia of parallel planar manipulators.^{2,17}

In applications where there is a heavy load on the platform, the vertical load will create a cantilever action on each of the links. Thus, there is a chance that it may limit the total vertical load that can be applied.

In this paper, the planar manipulator is conceived with non-planar (spatial) links. The top platform is raised above the base platform and the links are elevated to the top platform. The proposed design is expected to carry a higher payload and decrease the cantilever nature of the links. In nature, this design is more closely oriented toward the behavior of many living entities. The following illustrations depict the usage of inclined links (Fig. 1).

* Corresponding author. E-mail: ganeshm@mech.sastra.edu



Fig. 1. The figure depicts the usage of inclined links for carrying heavy loads. The inclined leg of the insect comes handy to maneuver the load of the insect body. In another case, inclined links of the hand are used to transmit high forces and accurate positioning without causing strain to the links.

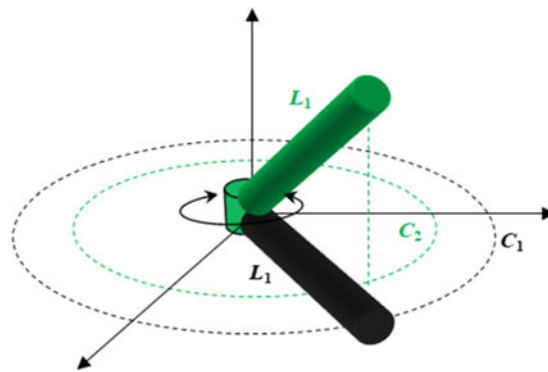


Fig. 2. Influence of inclined links on workspace/boundary singularities.

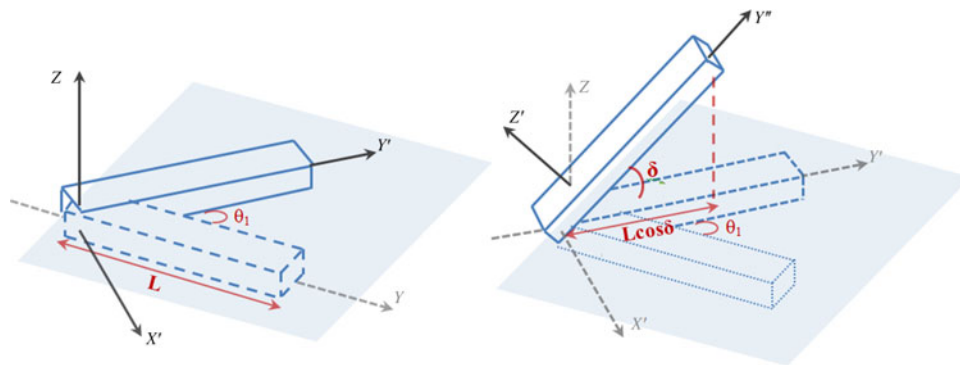


Fig. 3. Principle of inclination.

In practice, the load-bearing capability can be significantly improved with inclined links. It is also obvious that non-planar links are going to influence many other characteristics. For example, increasing the inclination angle improves the load-bearing capability and stiffness, but it may affect the workspace or Type I singularities. To drive home this point, a single link with a rotary joint R is illustrated (Fig. 2). The link shown in black color is placed in the XY plane. Another link in green is of the same size (L_1) and is inclined (the method of inclination is described in Fig. 3). Both the links are rotated around the Z axis. The planar link covers a work area C_1 , whereas the inclined (spatial) link covers C_2 .

It will be of the readers' interest to know the appropriate inclination angle which does not compromise any significant feature of the manipulator. The following features of the manipulator, such as the moment of inertia (MOI), stiffness, workspace, inertia forces and the moving mass of the manipulator are addressed in this article.

The existing mathematical models for the above parameters are tuned to reflect the changes in the model. Assuming cylindrical links (with circular cross section) for the manipulator's legs, the MOI and mass MOI of the links are determined. Conventional stiffness analysis is usually done by the Jacobian method which presumes the links as rigid elements and only active joint stiffness is considered.^{18,19} Here, the matrix structural approach is followed to study the proposed manipulator design, in which the links and top platform deflections are considered.^{20,21} In this article, the authors will be referring to the manipulator with Non-Planar Link Arrangement as 'NPLA manipulator' throughout the paper, for simple usage of language.

The new models for the above-mentioned kinematic parameters are obtained with generalized RR configuration. The proposed design is introduced in Section 2 with illustrations. A generalized mathematical model for RR configuration is developed for the parameters, such as workspace, stiffness and static forces in Section 3. A 3- $\bar{R}RR$ NPLA manipulator is taken as a case study to discuss the results of the analysis. It is shown that the models can also be developed with other manipulators (with non-planar links), such as 3- $\bar{P}RR$ and 3- $\bar{R}RR$, following the methodology described. The mathematical models of RR configuration are applied to 3- $\bar{R}RR$ parallel manipulator in Section 4, and the influence of the inclination angle is highlighted in Section 5. The results are discussed in comparison with the conventional manipulator in Section 6.

2. Proposed Design of Non-Planar Links

In the proposed design, the links are not in a single horizontal plane. The links are made non-planar by making it inclined about XY plane. The principle of elevating one of the links is shown in Fig. 3.

The first link of this mechanism is rotated by θ_1 degrees about Z axis. By this length L is shifted to Y' in XY plane. It is again rotated δ_1 degrees, but this time it is about X' axis. Thus Y' is shifted to Y'' . The same procedure is repeated for the other links of the leg. If L is projected unto the base plane, its projected length/magnitude will be $L\cos\delta$ (Fig. 3), while its original length remains L . Hence, the workspace for this model will be realized on a projected horizontal plane with the link lengths being the horizontal distance between any two joints.

Depending on the rotation of links about its X' axis (δ), the height of the top platform can be varied. This is to be decided based on requirement of kinematics parameters, such as workspace, stiffness and force transmission.

Therefore, for a particular inclination angle (δ), there are two link lengths – one is the projected link length ($L\cos\delta$) and the other is geometric link length (L). With the projected link length, the inverse kinematics, workspace and Jacobian are solved. For all the other characteristics such as mass of the manipulator in motion and stiffness, the geometric link length (L denoted in upper case) is used.

The proposal is conceived for the following configurations 3- $\bar{R}RR$, 3- $\bar{P}RR$ and 3- $\bar{R}RP$ and is illustrated in Table I. Although the links are made inclined to the horizontal plane, the rotary (or prismatic) joints axes remain perpendicular (or parallel as the case may be) to the plane of the base platform, which retains the planar motion of the end effector.

3. Static Modeling

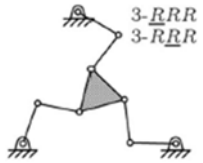
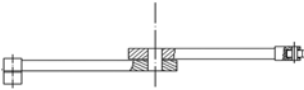
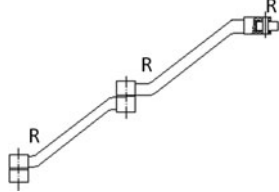
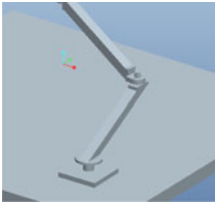
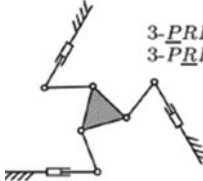
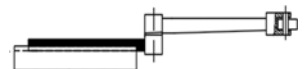
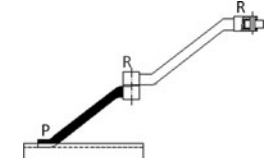

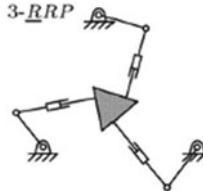
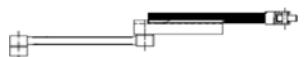
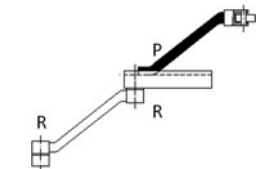

New mathematical models are required for studying the influence of the inclination angle in relation to the following parameters, such as workspace, MOI, stiffness, static forces and the moving mass of the manipulator.

3.1. Workspace of RR configuration

The workspace of the individual serial configuration (leg i) has been obtained geometrically. The non-planar links and its workspace are shown in blue color (Fig. 4).

To have a meaningful comparison of the PKMs, the workspace area should be same for both the manipulators, and hence the same link lengths are used. If the link lengths are taken as l_1 and l_2 for the conventional planar configuration, then the projected orthographic link lengths for NPL should also be taken as l_1 and l_2 . It is because the projected link lengths are only applicable for computing the workspace of NPL. These lengths are divided by $\cos\delta$ to get the original isometric link length.

Table I. The schematic of NPLA in individual leg of planar manipulators.

Planar manipulators	Single leg – planar links	Single leg – NPLA arrangement	Single leg – 3D model
 <p>3-RRR 3-RRR</p>			
 <p>3-PRR 3-PRR</p>			
 <p>3-RRP</p>			

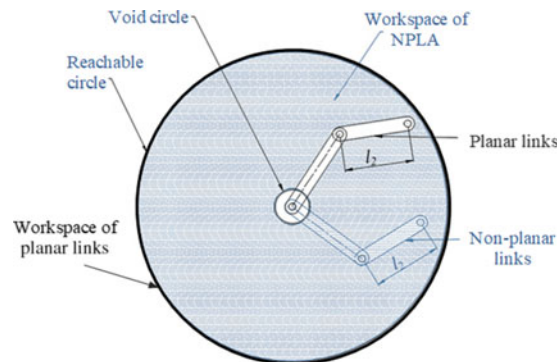


Fig. 4. Top view of the workspace of RR configuration.

3.2. Formulation of inertia tensor

The MOI of inclined link is different from that of the non-inclined link because the cross-section area about the vertical axis has changed.

Assuming cylindrical links (with circular cross section) for the manipulator legs, MOI for the links are determined. Let the cylindrical link be of radius R_c and length L is inclined about Y axis by an inclination angle (δ) as shown in Fig. 5.

In order to determine the MOI (second moment of area) about the Z axis (refer Fig. 5), the cross-section area of the inclined link in the XY plane is considered. The cross-section area is an ellipse with minor diameter equals R_c (along Y axis) and major diameter is $R_c/\cos\delta$ (along X axis), as the link is inclined about an angle δ .

$$\text{Area of cross section } A = \pi R_c \frac{R_c}{\cos \delta} \tag{1}$$

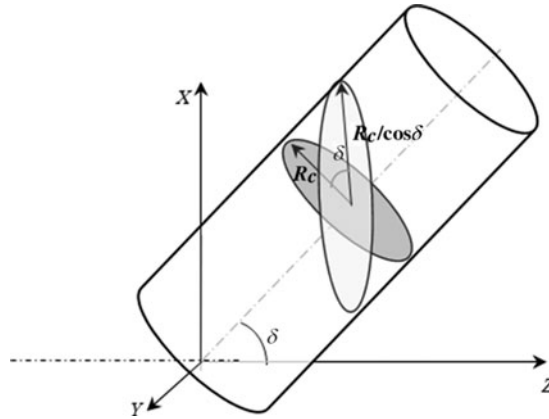


Fig. 5. A cylindrical link with circular cross section is inclined at δ° about Y axis. The inclined link has an elliptical cross section taken parallel to XY plane. This cross-section area is used for computing the MOI.

It can be noted that as $\delta \rightarrow 0^\circ$, the cross-section area is a circle and as $\delta \rightarrow 90^\circ$, the major diameter of ellipse $R_c / \cos \delta \rightarrow \infty$. It is not possible to obtain such elliptical cross section on links with finite length. That is, the maximum possible diameter (major) of elliptical cross section is limited by the link length L . Mathematically, $R_c / \cos \delta < L/2$ or in other words δ is limited by $2R_c/L$.

$$I_y = \frac{\pi R_c^4}{4 \cos^3 \delta}$$

$$\text{Polar moment of inertia } I_z = I_x + I_y = \pi \frac{R_c^4}{4} \left[\left(\frac{1}{\cos \delta} \right) + \left(\frac{1}{\cos \delta} \right)^3 \right] \tag{2}$$

Due to the presence of $\cos \delta$ term in (1) and (2), MOI increases nonlinearly with δ . However, δ is constrained by $2R_c/L$. Let us assume the link radius R_c to be 20 mm and the isometric link length to be 160 mm. Then the maximum possible inclination angle will be $\cos^{-1}(0.25) = 75.5^\circ$. Such large inclination angle increases the inertia to bending.

With the rise in MOI, the compliance of the links is very much reduced in comparison with the links of planar legs. The link flexibility is described by a full-scale 3D model²² that incorporates all deflections along and around X, Y, Z axes of the 3D Cartesian space

Stiffness matrix (S_M) Deflection Forces/moments

$$\frac{E}{L^3} \begin{bmatrix} A \cdot L^2 & 0 & 0 & 0 & 0 & 0 \\ 0 & 12I_z & 0 & 0 & 0 & -6I_z \cdot L \\ 0 & 0 & 12I_y & 0 & 6I_y \cdot L & 0 \\ 0 & 0 & 0 & \frac{G \cdot J \cdot L^2}{E} & 0 & 0 \\ 0 & 0 & 6 \cdot I_y \cdot L & 0 & 4I_y \cdot L^2 & 0 \\ 0 & -6I_z \cdot L & 0 & 0 & 0 & 4I_z \cdot L^2 \end{bmatrix} \begin{bmatrix} u_x \\ u_y \\ u_z \\ u_{\phi x} \\ u_{\phi y} \\ u_{\phi z} \end{bmatrix} = \begin{bmatrix} f_x \\ f_y \\ f_z \\ m_{\phi x} \\ m_{\phi y} \\ m_{\phi z} \end{bmatrix} \tag{3}$$

where A and I_y, I_z are the area and the second moments of the link cross section, J is the polar moment, L is the link length, and E and G are the Young and Coulomb modules of the material.

The terms A and I_z corresponds to the elliptical cross-section area of the non-planar links, which is represented by (1) and (2), respectively.

3.3. Stiffness modeling of RRR configuration

As mentioned in the introduction section, the matrix structural approach is adopted to study the stiffness of non-planar links. Since the links are assumed flexible, the inertia parameters obtained in the above section are substituted in the compliance matrix of link elements. The influence is studied in comparison to the planar parallel manipulator.

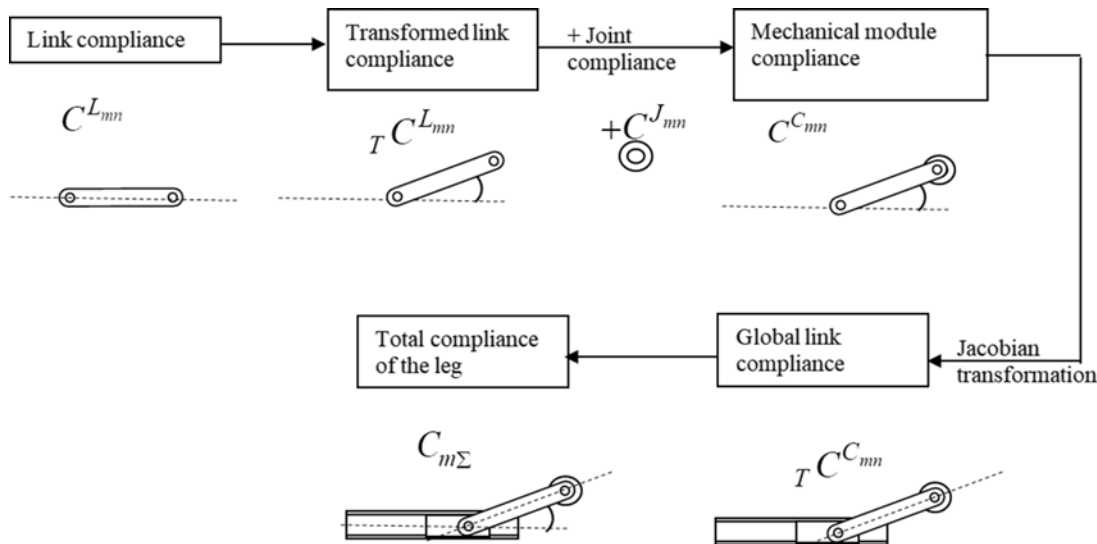


Fig. 6. The flow chart of methodology in determining the stiffness of a kinematic chain.

The following methodology as proposed by Nagai and Liu²² determines the stiffness model for a parallel mechanism. Here, the parallel mechanism is sub-divided into kinematic chains representing each leg. Each chain is further divided into mechanical modules in which the module represents a joint and its associated link.¹ Step-by-step procedure is given below and illustrated in Fig. 6.

- Step 1:** Links are assumed flexible. A 2D/3D spring model is used to determine the link compliance.
- Step 2:** The compliance of link $(j - 1)$ in leg i is expressed as $C^{Li(j-1)}$. This compliance undergoes rotational transformation ${}^{i(j-1)}R_{ij}$.

$$C^{Cij} = C^{Jij} + \begin{bmatrix} {}^{i(j-1)}R_{ij} & 0 \\ 0 & {}^{i(j-1)}R_{ij} \end{bmatrix}^{-1} C^{Li(j-1)} \begin{bmatrix} {}^{i(j-1)}R_{ij} & 0 \\ 0 & {}^{i(j-1)}R_{ij} \end{bmatrix} \quad (4)$$

${}^{i(j-1)}R_{ij}$ represents the rotational transformation between link $(j - 1)$ and j link of leg i .

- Step 3:** The compliance for the mechanical module C^{Cij} is transformed with regard to global reference by Jacobian matrix transformations. Assume displacement and orientation Δu_{ij} of frame F_{ij} with respect to top frame F_T . Its displacement is related to Jacobian matrix J_{ijT} .

$$\Delta u = J_{ijT}^{-1} \cdot \Delta u_{ij} \quad (5)$$

Using the rotational matrix, the following equation is obtained. ${}^B R_T$ refers to the rotational transformation of base frame F_B to top frame F_T

$${}^B \Delta u_T = \begin{bmatrix} {}^B R_T & 0 \\ 0 & {}^B R_T \end{bmatrix} J_{ijT}^{-1} \Delta u_{ij} = \begin{bmatrix} {}^B R_{ij} & {}^B R_{ij} [{}^{ij}P_T \times] \\ 0 & 1 \end{bmatrix} \Delta u_{ij} \quad (6)$$

- Step 4:** Steps 1–3 are repeated for each module. (Each joint and its associated link.)
- Step 5:** The compliance matrix hence obtained for each module is cumulatively added to give the total compliance of the kinematic chain.

The stiffness analysis is carried for RR configuration of the manipulator and extended for the other legs. The study is done in comparison to the planar links. For planar links, the modeling is based on 2D approach, whereas for non-planar links the modeling is by a 3D approach.

¹For a n th joint, $n - 1$ th link denotes the associated kinematic chain.

3.3.1. *Stiffness model for RR configuration – first mechanical module (first joint and its previous link)*. Since the first joint is an active joint, the compliance for the joint C^{J11} is taken as $diag(0, 0, S_{11}^{-1})$.

Considering the first link of leg 1

$$C^{C11} = {}_T C^{L10} + C^{J11} \tag{7}$$

where C^{C11} denotes the cumulative compliance (first joint and zeroth transformed link)

The transformed compliance $T^{C^{C11}} \times C^{C11}$ for this mechanical module (first joint and previous link together) is computed using (4) and (6)

$$T^{C^{C11}} = \begin{bmatrix} {}^B R_{ij} & {}^B R_{ij} [{}^{ij}P_T] \\ 0 & {}^B R_{ij} \end{bmatrix} \times C^{C11} \times \begin{bmatrix} {}^B R_{ij} & 0 \\ {}^B R_{ij} [{}^{ij}P_T] & {}^B R_{ij} \end{bmatrix} \tag{8}$$

3.3.2. *Second mechanical module (second joint and its previous first link)*. Links are assumed not to be rigid, so compliance for the links is obtained by materials science – structural analysis approach.

A 3D spring model is assumed for the conventional and the modified design to incorporate all deflections along and around X, Y and Z axes of the Cartesian space.

The compliance matrix is obtained by taking inverse of stiffness matrix in (3) (Section 3.2).

$${}_L C = (S_M)^{-1} \tag{9}$$

The compliance matrix in (9) represents the local stiffness matrix. It has to be transformed globally by rotational transformation as given below in (10). The method of rotation is shown in Fig. 7.

$$R_1 = \begin{bmatrix} C\theta_1 & -S\theta_1 & 0 \\ S\theta_1 & C\theta_1 & 0 \\ 0 & 0 & 1 \end{bmatrix} \times \begin{bmatrix} C\delta_1 & 0 & S\delta_1 \\ 0 & 1 & 0 \\ -S\delta_1 & 0 & C\delta_1 \end{bmatrix}. \tag{10}$$

Rotation about Z axis Rotation about Y axis

For the conventional planar manipulator, δ_1 is 0 (Fig. 7a).

The following (11) determines the transformed link compliance. Equations (9) and (10) are substituted in (11)

$$T^{C^{L11}} = \begin{bmatrix} R_1 & 0 \\ 0 & R_1 \end{bmatrix} \times {}_L C \times \begin{bmatrix} R_1^T & 0 \\ 0 & R_1^T \end{bmatrix} \tag{11}$$

The total stiffness C^{C12} is the combination of second joint stiffness and first link stiffness. Since the second joint is a passive joint, its compliance C^{J12} is neglected. Thus,

$$C^{C12} = T^{C^{L11}} + C^{J12} \tag{12}$$

Applying the previous method of transformation as in (8), $T^{C^{C12}}$ is obtained.

The same procedure is repeated for the *third mechanical module (third joint and its second link)*

$$C^{C12} = T^{C^{L11}} + C^{J12} \tag{13}$$

$$T^{C^{C13}} = \begin{bmatrix} {}^B R_{ij} & {}^B R_{ij} [{}^{ij}P_T] \\ 0 & 1 \end{bmatrix} C^{C13} \begin{bmatrix} {}^B R_{ij} & 0 \\ {}^B R_{ij} [{}^{ij}P_T] & 1 \end{bmatrix} \tag{14}$$

Adding (8), (12) and (14), the total compliance of $\bar{R}RR$ chain is given below.

$$C_{\Sigma} = {}_T C^{C11} + {}_T C^{C12} + {}_T C^{C13} \tag{15}$$

Taking inverse of (15), the stiffness of $\bar{R}RR$ chain is obtained.

$$S_{\Sigma} = C_{\Sigma}^{-1} \tag{16}$$

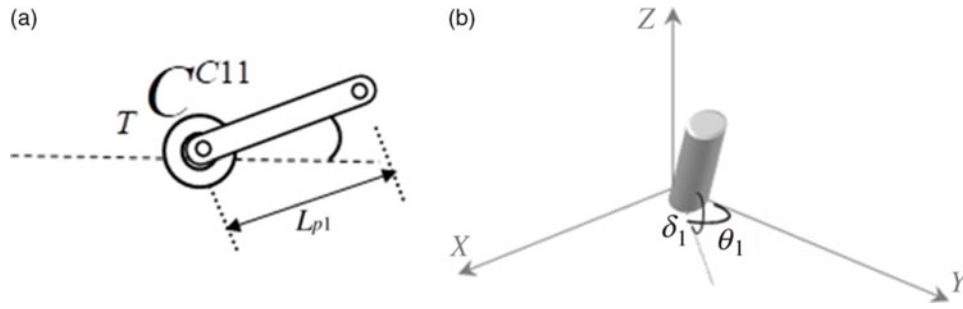


Fig. 7. (a) The active joint with first link (leg1) – conventional design; (b) the active joint with first link (leg 1) – modified design.

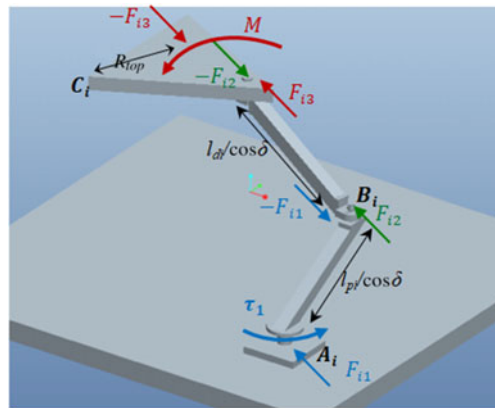


Fig. 8. Free body diagram of a single leg forces and moments.

3.4. Static force analysis

Static forces are studied by considering the free body diagram of the leg. The first member is the input link (proximal link); the second member as the coupler link (distal link). $l_{pi}/\cos\delta$ and $l_{di}/\cos\delta$ represent the proximal and distal link length for each leg i .

The joint torque τ_i provided to the input link of each leg i produces output forces f_x, f_y and f_z and moments m_{ϕ_x}, m_{ϕ_y} and m_{ϕ_z} on the mobile platform. The forces $(f_{i1}, -f_{i1})$ generated by the motor torque τ_i are the forces $(f_{i2}, -f_{i2})$ acting along the coupler link (Fig. 8). These forces in turn produce the moment in the top platform.²³ Hence, $f_{i1} = f_{i2} = f_{i3}$.

The forces exerted along the distal link l_{di} on each leg i can be related to the output forces, acting along the principal directions, as shown below:

$$\sum_{i=1}^n \frac{l_{di} \vec{f}_{i2}}{l_{di}} = [f_x \quad f_y \quad f_z]^T$$

$$\frac{1}{l_{di}} \begin{bmatrix} l_{d1}^x & l_{d2}^x & \dots & l_{dn}^x \\ l_{d1}^y & l_{d2}^y & \dots & l_{dn}^y \\ l_{d1}^z & l_{d2}^z & \dots & l_{dn}^z \end{bmatrix} \begin{bmatrix} f_{i2} \\ f_{i2} \\ \cdot \\ f_{i2} \end{bmatrix} = [f_x \quad f_y \quad f_z]^T \quad (17)$$

where l_{di}^x correspond to the i th leg distal link's x coordinates.

Summing all the moments applied to the top platform:

$$\sum_{i=1}^n \frac{\vec{e}_i \times \vec{f}_{i3}}{l_{di}} = [m_{\phi_x} \quad m_{\phi_y} \quad m_{\phi_z}]^T$$

where \vec{e}_i directed from C_i of leg i to the center of the platform. The magnitude is R_{top} :

$$\frac{1}{l_{di}} \begin{bmatrix} e_{1y}l_{d1}^z & e_{2y}l_{d2}^z & \dots & e_{ny}l_{dn}^z \\ -e_{1x}l_{d1}^z & -e_{2x}l_{d2}^z & \dots & -e_{nx}l_{dn}^z \\ e_{1x}l_{d1}^y - e_{1y}l_{d1}^x & e_{2x}l_{d2}^y - e_{2y}l_{d2}^x & \dots & e_{nx}l_{dn}^y - e_{ny}l_{dn}^x \end{bmatrix} \begin{bmatrix} f_{12} \\ f_{22} \\ \cdot \\ \cdot \\ f_{n2} \end{bmatrix} = \begin{bmatrix} m_{\varphi x} \\ m_{\varphi y} \\ m_{\varphi z} \end{bmatrix} \quad (18)$$

Similarly, summing all the moments applied to the input link $\tau_i = l_{pi} \times \vec{f}_{i1}$

$$\tau_i = \frac{f_{i2}}{l_{di}} [(l_{pi}^y l_{di}^z - l_{pi}^z l_{di}^y) - (l_{pi}^x l_{di}^z - l_{pi}^z l_{di}^x) + (l_{pi}^x l_{di}^y - l_{pi}^y l_{di}^x)]$$

Rewriting the above equation

$$f_{i2} = \frac{l_{di} \tau_i}{D_i}$$

Where

$$D_i = [(l_{pi}^y l_{di}^z - l_{pi}^z l_{di}^y) - (l_{pi}^x l_{di}^z - l_{pi}^z l_{di}^x) + (l_{pi}^x l_{di}^y - l_{pi}^y l_{di}^x)] \quad (19)$$

The output forces and the moments can be combined by grouping (17) and (18) onto a single matrix and substituted in (19) replacing the forces f_{i2} . Then, the resulting matrix in (20) represents the transformation of input torques to output forces.

$$\begin{bmatrix} f_x \\ f_y \\ f_z \\ m_{\varphi x} \\ m_{\varphi y} \\ m_{\varphi z} \end{bmatrix} = \begin{bmatrix} \frac{l_{d1}^x}{D_1} & \frac{l_{d2}^x}{D_2} & \dots & \frac{l_{dn}^x}{D_n} \\ \frac{l_{d1}^y}{D_1} & \frac{l_{d2}^y}{D_2} & \dots & \frac{l_{dn}^y}{D_n} \\ \frac{l_{d1}^z}{D_1} & \frac{l_{d2}^z}{D_2} & \dots & \frac{l_{dn}^z}{D_n} \\ \frac{e_{1y}l_{d1}^z}{D_1} & \frac{e_{2y}l_{d2}^z}{D_2} & \dots & \frac{e_{ny}l_{dn}^z}{D_n} \\ \frac{-e_{1x}l_{d1}^z}{D_1} & \frac{-e_{2x}l_{d2}^z}{D_2} & \dots & \frac{-e_{nx}l_{dn}^z}{D_n} \\ \frac{e_{1x}l_{d1}^y - e_{1y}l_{d1}^x}{D_1} & \frac{e_{2x}l_{d2}^y - e_{2y}l_{d2}^x}{D_2} & \dots & \frac{e_{nx}l_{dn}^y - e_{ny}l_{dn}^x}{D_n} \end{bmatrix} \begin{bmatrix} \tau_1 \\ \tau_2 \\ \cdot \\ \cdot \\ \tau_n \end{bmatrix} \quad (20)$$

4. Non-Planar Links in 3-RRR Parallel Manipulator

A planar symmetric 3-DOF parallel manipulator (3-RRR) is shown in Fig. 9. R_{base} and R_{top} define the size of the fixed platform and mobile platform, respectively; l_{p1} and l_{d1} are the lengths of the first and second links of the three legs, respectively. The link lengths are indeed the projected link lengths and they are divided by $\cos\delta$ to get the isometric link lengths. Due to symmetric condition, for $i = 1, 2, 3$; $l_{pi} = l_p$; $l_{di} = l_d$.

The output forces obtained in (20) provide the output transmission capability. Indeed, the parallel manipulators also possess input transmission capability. Hence, an input transmission index (ITI) is determined along with the output transmission index (OTI).

For an individual RRR leg consisting of three joints, the transmission wrench is a pure torque. Thus, the ITI is obtained as the absolute of the sine of angle between the two Z planes,²⁴ each plane containing the input link and the coupler link, respectively. Referring to Fig. 9, the

$$ITI = |\sin(\theta_2)_i| \quad (21)$$

and the

$$OTI = |\sin(\theta_3)_i| \quad (22)$$

A local transmission index (LTI) captures both the indices, by finding the minimum of the two indices.

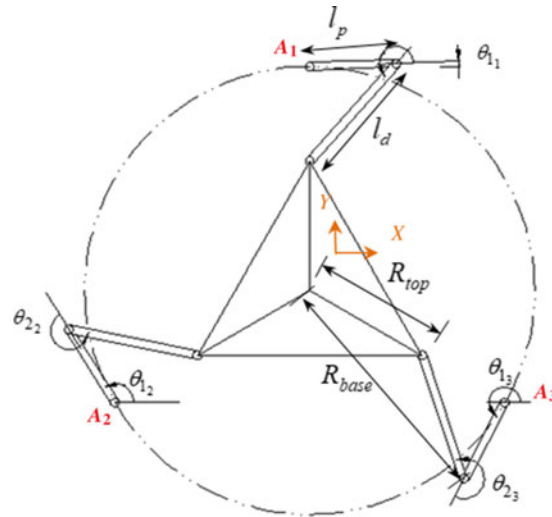


Fig. 9. Top view schematic of 3- $\bar{R}RR$ manipulator at home position. It shows the manipulator parameters, such as link lengths, top platform size and joint angle notations. The proximal link is denoted as l_p and the distal link as l_d . γ denotes the angle of proximal link of leg i .

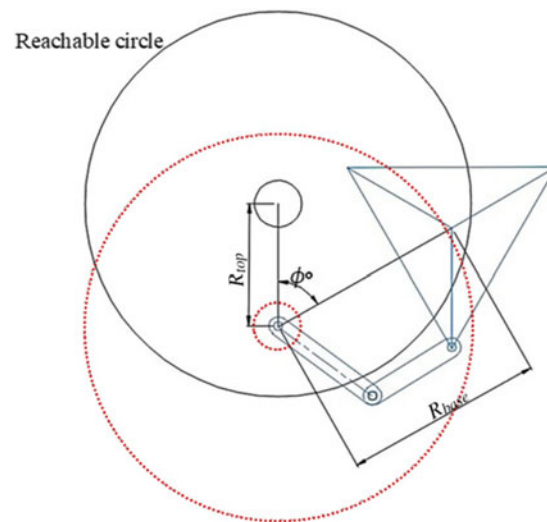


Fig. 10. Method of workspace determination.

4.1. Workspace of 3- $\bar{R}RR$ parallel manipulator

The workspace of the individual $\bar{R}RR$ leg i is represented by reachable circle whose radius is $l_{p1} + l_{d1}$. The center of each individual reachable circle is initially at the corresponding base platform coordinates A_1, A_2, A_3 (Fig. 9). For finding the mutual workspace of all the three legs, the individual workspace of each leg is translated from their base platform to a vector v_i of magnitude equivalent to the radius of the mobile platform R_{top} , along the direction of mobile platform orientation ϕ° (Fig. 10).

The void circle and the reachable circle (of leg 2) are shown as red dotted circles, before the translation and black circles, after the translation by a magnitude R_{top} . The reachable circles C_1, C_2 and C_3 corresponding to each leg are translated, and the obtained mutual workspace is denoted as M_1, M_2 and M_3 in Fig. 11.

The mutual workspace area is approximated to be a circle of radius R_w , passing through the intersection points P_1, P_2 and P_3 (Fig. 11). The intersection points are indeed the points of intersection of the medians (of base triangle) with the individual reachable circles.

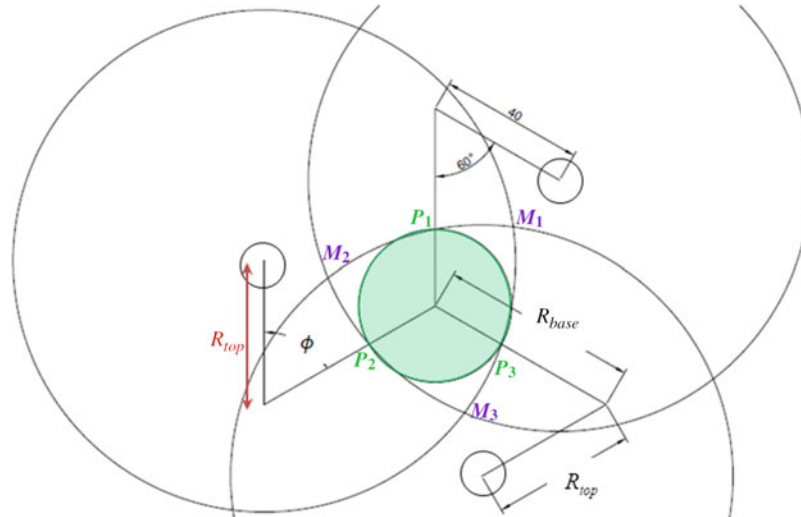


Fig. 11. Mutual workspace area of 3-RRR manipulator.

Solving by geometrical method, the radius R_w of the workspace circle is obtained.

$$R_w = R_d^2 + (l_p + l_d)^2 + 2 \times R_d (l_p + l_d) \cos \left(120 + \sin^{-1} \left(\frac{R_d \sin (120 + \tan^{-1} X)}{\cos \delta} \right) \right) \quad (23)$$

where

$$R_d = R_{base}^2 + R_{top}^2 + 2 \times R_{base} R_{top} \cos \phi$$

$$X = \frac{R_{top} \sin \phi}{R_{base} - R_{top} \cos \phi}$$

$$l_p = l_{p1} = l_{p2} = l_{p3}; l_d = l_{d1} = l_{d2} = l_{d3}$$

4.2. Homogenous stiffness matrix of 3-RRR parallel manipulator

The stiffness matrix given by (16) is used for solving the stiffness of the manipulator and is expressed as (24). The stiffness values have mixed dimensionality as shown below.

$$\begin{bmatrix} F \\ M \end{bmatrix} = \begin{bmatrix} K_{TT} & K_{TR} \\ K_{RT} & K_{RR} \end{bmatrix} \begin{bmatrix} U_T \\ U_R \end{bmatrix} \quad (24)$$

where

$$F = [f_x \quad f_y \quad f_z]^T; M = [m_{\phi x} \quad m_{\phi y} \quad m_{\phi z}]^T; U_T = [U_x \quad U_y \quad U_z]^T; U_R = [U_{\phi x} \quad U_{\phi y} \quad U_{\phi z}]^T$$

K_{TT} is translational stiffness sub-matrix (N/m); K_{TR} is coupling stiffness sub-matrix (N); K_{RR} is rotational stiffness sub-matrix (Nm).

For stiffness matrix index, either condition number or eigenvalues are computed. The eigenvalue computation is meaningful only if the stiffness matrix has homogenous units.

The unit-inconsistent matrix in (24) is partitioned into homogeneous translational and rotational components.²⁵ This is done by mapping the deflections $U = [U_T \quad U_R]^T$ to two dimensionless space $\psi = [\psi_T \quad \psi_R]^T$ and $\gamma = [\gamma_T \quad \gamma_R]^T$. This is possible by the eigen decomposition property, as given below.

Consider an ellipsoid $\{U_T | U_T^T A U_T = 1\}$. Since $K_{TT}^T K_{TT}$ is a real symmetric matrix, matrix A in the ellipsoid can be replaced by $K_{TT}^T K_{TT}$. By eigen decomposition, $K_{TT}^T K_{TT} = S_d \Lambda S_d^T$ where S is

an orthogonal matrix with the eigenvectors of $K_{TT}^T K_{TT}$ and the diagonal matrix Λ contains the eigenvalues of $K_{TT}^T K_{TT}$.

Then, the ellipsoid equation can be rewritten as:

$$U_T^T (S_d \Lambda S_d^T) U_T = (S_d^T U_T)^T \Lambda (S_d^T U_T) = \psi_T^T \Lambda \psi_T \tag{25}$$

where $\psi_T = S_d^T U_T$.

It simply means that ψ_T and U_T shares the same eigenvalues and same axes for the ellipsoids. However, the units are different. In general, $U = S\psi$ where $S = [S_d \ S_\varphi]$ consists of orthogonal matrices S_d and S_φ , whose columns are eigenvectors of $K_{TT}^T K_{TT}$ and $K_{TR}^T K_{TR}$, respectively. Similarly, $U = T_\gamma$ where T_d and T_φ constitute of eigenvectors of $K_{RT}^T K_{RT}$ and $K_{RR}^T K_{RR}$, respectively.

Now, (24) can be decoupled to

$$F = [K_{TT} S_d \quad K_{TR} S_\varphi] \begin{bmatrix} \psi_T \\ \psi_R \end{bmatrix} \tag{26}$$

$$M = [K_{RT} T_d \quad K_{RR} T_\varphi] \begin{bmatrix} \gamma_T \\ \gamma_R \end{bmatrix} \tag{27}$$

$[K_{TT} S_d \quad K_{TR} S_\varphi] = K S_T$ is a dimensionally homogeneous coefficient matrix of units N. Similarly, $[K_{RT} T_d \quad K_{RR} T_\varphi] = K S_R$ is a dimensionally homogeneous coefficient matrix of units Nm. $K S_T K S_T^T$ results in a 3×3 translational stiffness matrix, whose eigenvalues form an ellipse corresponding to the translational portion of stiffness.

5. Design Optimization

From the above study, it can be understood that increasing the inclination angle improves the inertia to bending and stiffness, but it affects either the *moving mass of the manipulator* or the *workspace*. For example, inclination angle as high as 80° improves the inertia (Section 3.2), but the size of the link ($l_p / \cos 80^\circ$) increases by 600% compared to the conventional manipulator and hence the mass of the manipulator rises. Hence, it will be of the readers' interest to know the appropriate inclination angle which does not compromise any feature of the manipulator.

Another parameter which is very influential in the parallel manipulator optimization is the orientation of the mobile platform. This parameter influences the *LTI* and the *workspace* of the manipulator. The influence of this parameter is briefly discussed in this design optimization process.

5.1. Multi-Objective Design Optimization (MODO) using genetic algorithm

In general, for any application, desirable workspace without singularities becomes highest order of importance among the objectives. Hence, the workspace is applied as a constraint. All the other objectives are decided by the user according to his requirements. In this particular example, the *moving mass of the manipulator*, *LTI* and the *stiffness index* are taken as objectives. They are assigned as objectives to the MODO problem.

gamultiobj solver (a multi-objective optimization using genetic algorithm solver) of MATLAB tool is used in this optimization problem.²⁶

5.1.1. Design objectives and constraints for optimizing 3-RRR manipulator.

1. The moving mass of the manipulator = mass of six links + mass of the platform

$$M_{RRR} = 3 \times \pi R_c^2 \frac{l_p}{\cos \delta} \vartheta + 3 \times \pi R_c^2 \frac{l_d}{\cos \delta} \vartheta + \pi R_{top}^2 t \vartheta \tag{28}$$

where ϑ is the density of the material. For steel, the value is 7850 kg/m^3 and for aluminum it is 2700 kg/m^3 ; R_c is the radius of link's circular cross section; R_{top} is the radius of the top platform; and t is the thickness of the top platform.

Table II. Summary of modified expressions.

Parameter	Expression
Moment of inertia of individual link	$I_Z = \pi \frac{R_c^4}{4} \left[\left(\frac{1}{\cos \delta} \right) + \left(\frac{1}{\cos \delta} \right)^3 \right]$
Mass moment of inertia	$I_{ZZ} = \frac{M_L R_c^2}{4} \left(\frac{1}{\sin^2 \delta} \right) + \frac{M_L L^2}{3} (\sin^2 \delta)$
The moving mass of 3- $\bar{R}RR$ mechanism	$M_{RRR} = 3 \times \pi R_c^2 \frac{l_p}{\cos \delta} \vartheta + 3 \times \pi R_c^2 \frac{l_d}{\cos \delta} \vartheta + \pi R_{top}^2 t \vartheta$
Workspace of 3- $\bar{R}RR$ mechanism	$R_d^2 + (l_p + l_d)^2 + 2 \times R_d (l_p + l_d) \cos \left(120 + \sin^{-1} \left(\frac{R_d \sin(120 + \tan^{-1} X)}{\cos \delta} \right) \right)$

2. LTI is the minimum of the two indices namely *ITI* and *OTI*, obtained from (21)

$$LTI = \min(ITI, OTI) \tag{29}$$

3. The eigenvalues E_x, E_y and E_z are computed from the translational portion $KS_T KS_T^T$ obtained in Section 4.2. Similarly, eigenvalues $E_{\phi x}, E_{\phi y}$ and $E_{\phi z}$ are computed from the rotational portion matrix $KS_R KS_R^T$.

The stiffness index is given by

$$S_I = \min \left(\sqrt{E_x}, \sqrt{E_y}, \sqrt{E_z}, \sqrt{E_{\phi x}}, \sqrt{E_{\phi y}}, \sqrt{E_{\phi z}} \right) \tag{30}$$

The constraints are as follows:

1. The geometric constraint is

$$L + R_{top} \geq \frac{R_{base}}{2} \tag{31}$$

where R_b is the radius of the base platform.

2. The workspace constraint is provided by (23). Since the order of the symmetry group of the manipulator is 6, then the searching range for the orientation angle ϕ is reduced from 0 to $\frac{2\pi}{6}$.^{27,28}

5.2. Multi-objective optimization problem statement

The multi-objective design optimization problem of the model is reinstated as: *To find the optimum design variables X in order to minimize the moving mass of the mechanism and to maximize its stiffness and LTI in XY plane subject to geometric, kinematic and workspace constraints.*

Mathematically, the problem can be summarized as:

minimize $f_1(x) = M_{RRR}$

maximize $f_2(x) = LTI$ and S_I

Over $X = [l_p \quad l_d \quad R_{top} \quad \delta \quad \varphi]$ subject to $g1 : L + R_{top} \geq \frac{R_{base}}{2}$

$X_{lb} = [100 \quad 100 \quad 120 \quad 0 \quad 0]$ $g2 : R_w \geq 80$

$X_{ub} = [200 \quad 200 \quad 150 \quad 70 \quad 60]$

The limits for the inclination angle is chosen between 0 and 70 because of the constraint discussed in Section 3.2

6. Results and Analysis

Summary of all the static characteristic expressions discussed in Section 3 and Section 4 are tabulated in Table II.

Table III. The pareto front solutions for solution SET 1 of the variables (decision space).

Solution	Decision space (variables)					Objectives	
	Link length proximal l_p (mm)	Link length distal l_d (mm)	Radius top platform R_{top} (mm)	Inclination angle δ (degree)	Orientation angle ϕ (degree)	Moving mass M_{RRR} (kg)	Smallest eigenvalue (N)
f_6	104	173	122	37	3	11.7	6.4×10^6
f_7	105	171	122	39	4	11.9	5.0×10^6
f_8	105	171	122	38	4	11.8	5.0×10^6
f_{26}	105	173	122	38	4	11.8	6.2×10^6

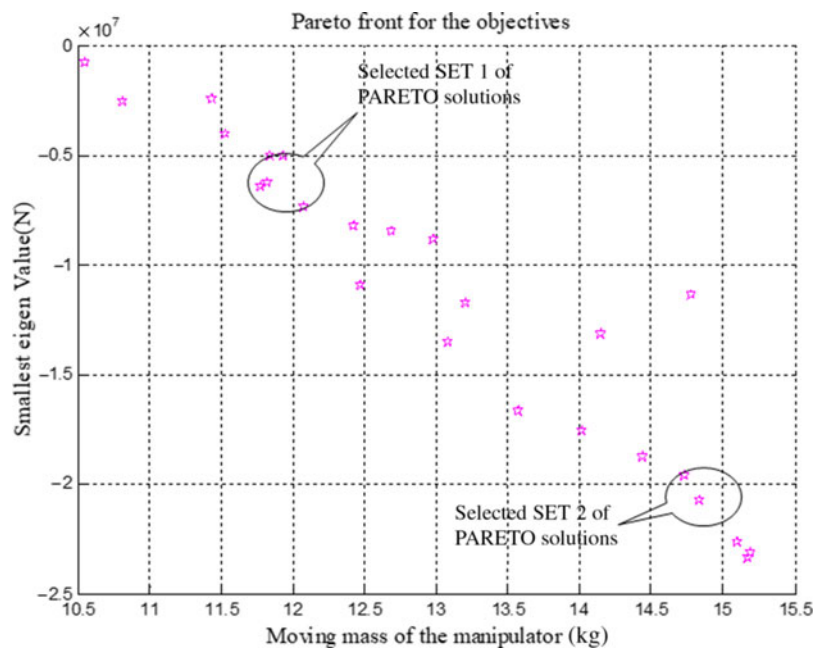


Fig. 12. Pareto front for the objectives – the moving mass and stiffness along Z axis.

The inclination angle influences the static characteristics which can be inferred by the presence of $\cos\delta$ term or $\sin\delta$ term in these expressions in Table II. As discussed in Section 3.2, the inertia to bending moment is significantly increased which favors the stiffness of the manipulator.

6.1. Optimization results

Two sets namely SET 1 and SET 2 are selected from the solutions of the multi-objective optimization, as shown in Fig. 12.

The optimized variables and the corresponding function values (objective values) are listed in Tables III and IV for the selected SET 1 and SET 2, respectively. The SET 1 is chosen to highlight the low moving mass of the manipulator, whereas the SET 2 highlights the high stiffness value of the manipulator.

The stiffness value for SET 2 is greater than SET 1 by 15×10^6 N due to the influence of the inclination angle but with a compromise in the moving mass, a relatively higher ‘moving mass’ compared to SET 1.

The highlighting difference between the two tables is the inclination angle and the size of the distal link. It can be inferred that the optimal inclination angle varies from 30° to 60° .

Table IV. The pareto front solutions for solution SET 2.

Solution	Decision space (variables)					Objectives	
	Link length proximal l_p (mm)	Link length distal l_d (mm)	Radius top platform R_{top} (mm)	Inclination angle δ (degree)	Orientation angle ϕ (degree)	Moving mass M_{RRR} (kg)	Smallest eigenvalue (N)
f_{10}	104	158	124	61	6	14.8	2.0×10^7
f_{11}	105	158	124	61	5	14.8	1.8×10^7
f_{12}	105	158	123	61	6	14.8	1.2×10^7
f_{19}	105	158	124	58	6	14.2	1.3×10^7

Table V. Eigenvalues from the translation and rotational portion.

Eigenvalue E	Inclination angle δ (degree)		
	$\delta = 0^\circ$	$\delta = 35^\circ$	$\delta = 70^\circ$
E_x	0.013×10^8	0.027×10^8	0.452×10^8
E_y	0.023×10^8	0.033×10^8	0.547×10^8
E_z	0.229×10^8	0.310×10^8	2.784×10^8
E_{ϕ_x}	0.371×10^8	0.395×10^8	0.162×10^8
E_{ϕ_y}	1.002×10^8	0.890×10^8	0.227×10^8
E_{ϕ_z}	4.450×10^8	4.657×10^8	3.133×10^8

6.2. Stiffness results

The decoupled stiffness matrix as given in (26) and (27) of Section 4.2 is generated for one set of the optimized parameters in Table IV. The eigenvalues for $KS_T KS_T^T$ (translational portion of stiffness) and $KS_R KS_R^T$ (rotational portion of stiffness matrix) are displayed in Table V. In order to have a comparison study, the eigenvalues are obtained for inclination angle (δ) ranging from 0° to 70° .

Comparing the eigenvalues above, it is deduced that the modified design (with large inclination angle) yields translational stiffness values that are 10 times higher compared to the conventional design. However, the modified design has marginally low rotational stiffness compared to the conventional design.

The condition number for $KS_T KS_T^T$ is plotted against the inclination angle for the same set of configuration.

From the Fig. 13, it can be noted that the condition number is low (close to 2) for an inclination angle of 30° – 60° and this result is in coherence with the optimization result.

The smallest eigenvalue is plotted for the entire workspace. The minimum value and the maximum value (of the smallest eigenvalue) over the entire workspace are indicated in Fig. 14. The increase in the minimum as well as the maximum value for the modified 3-RRR version is very promising in comparison with the conventional manipulator.

The minimum value for the modified 3-RRR version is 6.6134×10^5 N, which is six times higher compared to the conventional manipulator's minimum value 1.1051×10^5 N. Similarly, the maximum value for the modified 3-RRR version is 3.3 times higher compared to the conventional manipulator.

6.3. Application of non-planar (spatial) links

Generally, planar mechanisms find their applications in machining applications. With the non-planar links, the payload limitation can be overcome. As it improves the translational stiffness, it is highly applicable to simulations involving translational motions. For example, one such application is the 6-DOF shake table (Fig. 15) developed by the authors because the earthquake motion predominantly involves translation motion.

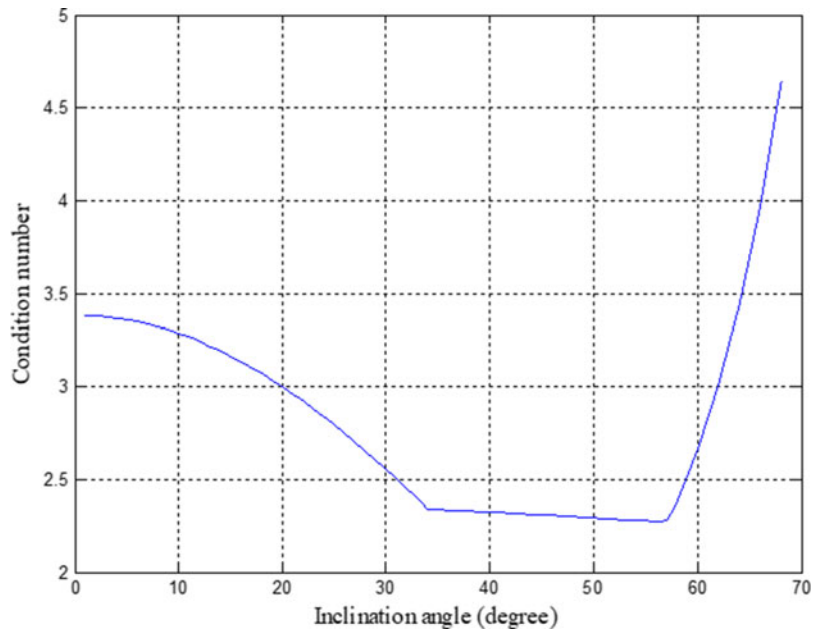


Fig. 13. Condition number of translational stiffness portion.

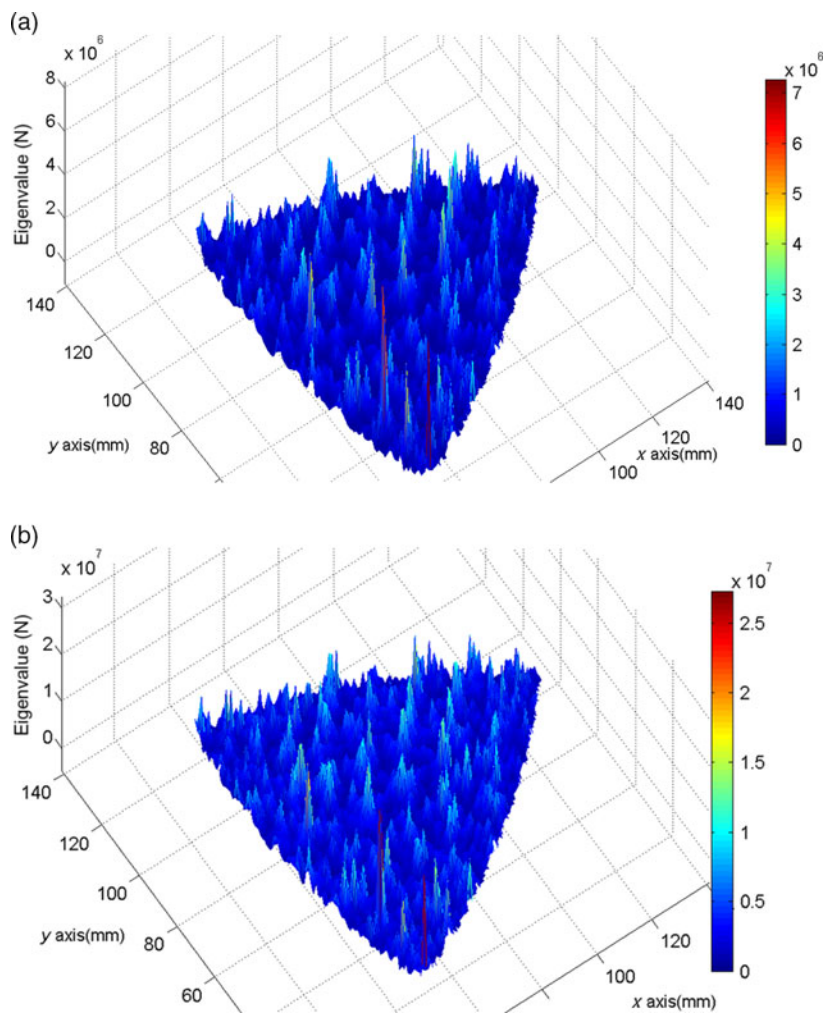


Fig. 14. Smallest eigenvalue map in XY plane for (a) conventional 3- \bar{R} RR manipulator and (b) modified 3- \bar{R} RR manipulator.

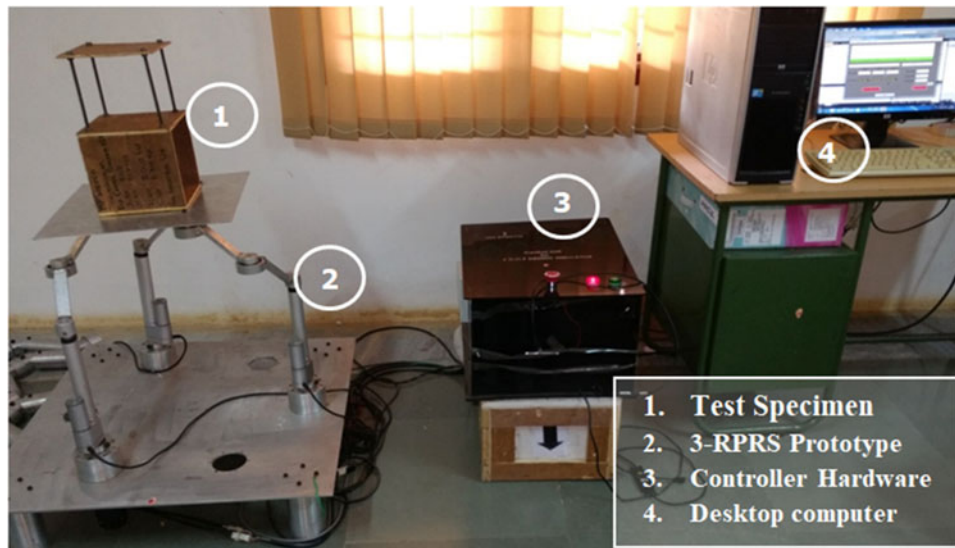


Fig. 15. A 6-DOF shake table based on three-legged RPRS topology.

7. Conclusion

In this paper, non-planar links are proposed for a class of planar parallel manipulators by which the distance between the mobile platform and base platform is raised. NPLA is implemented with the expectation of increasing the payload capacity and decreasing the cantilever nature of the links. This is supported by the improvement in the static characteristics behavior of non-planar links.

The following specific conclusions can be drawn:

1. The formulated inertia tensor for the modified links substantiates the improvement of stiffness of the modified links of legs.
2. Results show that the translational portion of stiffness matrix is 10 times higher compared to the conventional planar parallel manipulator.
3. The stiffness matrix is well conditioned for an inclination (δ) between 30° and 60° .
4. With the rise in inclination angle, there is a marginal decline in rotational stiffness and rise in moving mass of the manipulator.

An optimal inclination angle δ was determined which maximizes the LTI index, stiffness and minimizes the moving mass of the manipulator while fulfilling the workspace area requirement.

Acknowledgments

The project is funded by DST, India, project no. SB/S3/MMER/0013/2014, to which the authors like to express their gratitude. The authors also express their gratitude to Dr. Badri Narayanan for his support in stiffness modeling.

References

1. C. Gosselin, *Kinematic Analysis, Optimization and Programming of Parallel Robotic Manipulators* (McGill University, Montréal, Canada, 1988).
2. B. Kang, J. Chu and J. K. Mills, "Design of High Speed Planar Parallel Manipulator and Multiple Simultaneous Specification Control," *Proceedings 2001 ICRA. IEEE International Conference on Robotics and Automation*, vol. 3 (2001) pp. 2723–2728.
3. J.-P. Merlet, C. M. Gosselin and N. Mouly, "Workspace of planar parallel manipulators," *Mech. Mach. Theory* **33**(1–2), 7–20 (1998).
4. C. M. Gosselin and J. Martin, "Determination of the workspace of planar parallel manipulators with joint limits," *Rob. Auton. Syst.* **17**(3), 129–138 (1996).
5. J. P. Merlet, "Direct kinematics of planar parallel manipulators," *Proc. IEEE Int. Conf. Rob. Autom.* **4**, 3744–3749 (1996).
6. H. Yu, B. Li, X. Yang and Y. Hu, "Structural synthesis and variation analysis of a family of 6-DoF parallel mechanisms with three limbs," *Int. J. Rob. Autom.* **25**(2), 121 (2010).

7. G. R. Pennock and D. J. Kassner, "Kinematic analysis of a planar eight-bar linkage: Application to a platform-type robot," *J. Mech. Des.* **114**(1), 87–95 (1992).
8. D. Chablat and P. Wenger, "The Kinematic Analysis of a Symmetrical Three-Degree-of-Freedom Planar Parallel Manipulator," *CISM-IFToMM Symposium on Robot Design, Dynamics and Control, Montreal* (2004).
9. D. Chablat, P. Wenger and J. Angeles, "Working Modes and Aspects in Fully-Parallel Manipulators," *IEEE International Conference on Robotics and Automation* (1998) pp. 1964–1969.
10. K. H. Hunt, "Structural kinematics of in-parallel-actuated robot-arms," *J. Mech. Trans. Autom. Des.* **105**(4), 705–712 (1983).
11. M. H. R. Daniali and J. Angeles, "Singularity analysis of planar parallel manipulators," *Mech. Mach. Theory* **30**(5), 665–678 (1995).
12. R. Rizk, M. Munteanu, J. Fauroux and G. Gogu, "A Semi-analytical Stiffness Model of Parallel Robots from the Isoglide Family via the Sub-structuring Principle," *Proceedings of 12th IFToMM World Congress* (2007)
13. M. Arsenault and R. Boudreau, "The synthesis of three-degree-of-freedom planar parallel mechanisms with revolute joints (3-RRR) for an optimal, singularity-free workspace," *J. Rob. Sys.* **21**(5), 259–274 (2004).
14. F. Gao, X.-J. Liu and X. Chen, "The relationships between the shapes of the workspaces and the link lengths of 3-DOF symmetrical planar parallel manipulators," *Mech. Mach. Theory* **36**(2), 205–220 (2001).
15. C. M. Gosselin and J. Angeles, "The optimal kinematic design of a planar three-degree-of-freedom parallel manipulator," *J. Mech. Trans. Autom.* **110**(3), 35–41 (1988).
16. G. Alici and B. Shirinzadeh, "Optimum dynamic balancing of planar parallel manipulators based on sensitivity analysis," *Mech. Mach. Theory* **41**(12), 1520–1532 (2006).
17. G. Clement, "Stiffness mapping for parallel manipulators," *IEEE Trans. Rob. Autom.* **6**(3), 377–382 (1990).
18. J. Wang, C. Wu and X.-J. Liu, "Performance evaluation of parallel manipulators: Motion/force transmissibility and its index," *Mech. Machine Theory* **45**(10), 1462–1476 (2010).
19. B. S. El-Khasawneh and P. M. Ferreira, "Computation of stiffness and stiffness bounds for parallel link manipulators," *Int. J. Mach. Tools Manuf.* **39**(2), 321–342 (1999).
20. A. Pashkevich, A. Klimchik and D. Chablat, "Enhanced stiffness modeling of manipulators with passive joints," *Mech. Mach. Theory* **46**(5), 662–679 (2011).
21. Y. Lu, J. J. Yu, L. W. Chen, X. L. Zhang, J. D. Han and C. P. Sui, "Stiffness and elastic deformation of a 3-leg 5-dof parallel manipulator with one composite leg," *Int. J. Rob. Autom.* **29**(1), 23–31 (2014).
22. K. Nagai and Z. Liu, "A Systematic Approach to Stiffness Analysis of Parallel Mechanisms," *IEEE International Conference on Robotics and Automation, ICRA 2008* (2008) pp. 1543–1548.
23. L. W. Tsai, *Robot Analysis: The Mechanics of Serial and Parallel Manipulators* (John Wiley & Sons, New York, 1999).
24. A. Klimchik, A. Pashkevich, S. Caro and D. Chablat "Stiffness matrix of manipulators with passive joints: Computational aspects," *IEEE Trans. Rob.* **28**(4), 955–958 (2011).
25. M. Anson, A. Aliakbar and K. Venkat, "Orientation workspace and stiffness optimization of cable-driven parallel manipulators with base mobility," *J. Mech. Rob.* **9**(3), 031011 (2017).
26. R. T. Marler and J. S. Arora, "Survey of multi-objective optimization methods for engineering," *Struct. Multidiscip. Optim.* **26**(6), 369–395 (2004).
27. J.-S. Zhao, F. Chu and Z.-J. Feng, "Symmetrical characteristics of the workspace for spatial parallel mechanisms with symmetric structure," *Mech. Mach. Theory* **43**(4), 427–444 (2008).
28. J. S. Zhao, Z. Feng, F. Chu and N. Ma. *Advanced Theory of Constraint and Motion Analysis for Robot Mechanisms* (Academic Press, 2013).

Appendix: Symbols and Notations

δ	Inclination angle
θ_{1_1}	Angle made by l_{p1} with the horizontal
θ_{2_1}	Angle made by l_{d1} with the proximal link of leg 1
$T^{C^{Lij}}$	Transformed link compliance for link j of leg i
C^{Jij}	Joint compliance for joint j of leg i
C^{Cij}	Cumulative compliance (joint j and j^{-1} link together)
$T^{C^{Cij}}$	Transformed cumulative compliance for joint j of leg i
$C_{i\Sigma}$	The total compliance of leg i (all the links and joints together)
C_{2_1}, S_{2_1}	$\cos(\theta_{2_1}), \sin(\theta_{2_1})$ of leg 1
C_{2-1_1}, S_{2-1_1}	$\cos(\theta_{2_1} - \theta_{1_1}), \sin(\theta_{2_1} - \theta_{1_1})$ of leg 1
E	Young's modulus of the material

E_x, E_y, E_z	Eigenvalues of the translational portion of stiffness matrix
f_{i2}	Static force acting along the coupler link of leg i . Coupler link is the second link
f_x	Static force at the end effector along the X axis
F	Force vector acting at the end effector
G	Coulomb modulus of the material
$I_y I_z$	Second moments of the link
J_{3R}	Jacobian of 3- $\bar{R}RR$ parallel manipulator
L	Original/isometric length of link
l_{1i} or l_{pi}	Proximal link to motor with length L_1 of leg i
l_{2i} or l_{di}	Distal link to motor with length L_2 of leg i
$l_{pi}^x, l_{pi}^y, l_{pi}^z$	Length of proximal link in X, Y and Z direction, respectively
$l_{di}^x, l_{di}^y, l_{di}^z$	Length of distal link in X, Y and Z direction, respectively
M_{RRR}	The moving mass of the manipulator
$m_{\phi_x}, m_{\phi_y}, m_{\phi_z}$	Moments applied to the mobile platform about X, Y and Z axes
R_c	Radius of links cross section
R_{top}	Radius of the circle which circumscribes the triangular mobile platform
R_{base}	Radius of the circle which circumscribes the triangular base platform
${}^{i(j-1)}R_{ij}$	Rotational transformation between link $(j - 1)$ and j link of leg i
U_x, U_y, U_z	The displacements along X, Y and Z axes, respectively